Investigation of Aromatic/Aliphatic Polyimides as Dispersants for Single Wall Carbon Nanotubes

Donavon M. Delozier,† Kent A. Watson,† Joseph G. Smith, Jr.,‡ Thomas C. Clancy,† and John W. Connell*,‡

National Institute of Aerospace, 100 Exploration Way, Hampton, Virginia 23666-6147, and NASA Langley Research Center, Advanced Materials and Processing Branch, Hampton, Virginia 23681-2199

Received August 18, 2005; Revised Manuscript Received January 10, 2006

ABSTRACT: Novel aromatic/aliphatic polyimides were prepared from 2,7-diamino-9,9′-dioctylfluorene (AFDA) and aromatic dianhydrides. Upon investigating the effectiveness of these polyimides for debundling single wall carbon nanotubes (SWNTs) in solution, three were discovered to aid in the dispersion of SWNTs in *N,N*-dimethylacetamide (DMAc). Two of these polyimides, one from 3,3′,4,4′-oxydiphthalic anhydride (ODPA) and one from symmetric 3,3′,4,4′-biphenyltetracarboxylic dianhydride (s-BPDA), were used to prepare nanocomposites. Homogeneous polyimide/SWNT suspensions from both polymers were used in the preparation of films and fibers containing up to 1 wt % SWNTs. The samples were thermally treated to remove residual solvent, and the films were characterized for SWNT dispersion by optical and high-resolution scanning electron microscopy (HRSEM). Electrical and mechanical properties of the films were also determined. Electrospun fibers were examined by HRSEM to characterize SWNT alignment and orientation.

1. Introduction

Polymer systems containing dispersed nanoparticles represent a class of materials with a combination of properties generally not obtainable in conventional polymers. Carbon nanotubes, especially single wall carbon nanotubes (SWNTs), are among the most attractive of all nanoparticles due to their high aspect ratio and desirable mechanical and electrical properties. The addition of SWNTs to polymers can change select material properties even at low loading levels when properly dispersed. For example, adding small amounts of SWNTs to insulating polymers such as polyimides can impart electrical conductivity while having little effect on the appearance and optical and mechanical properties of the material. This has been demonstrated in recent efforts to develop transparent, flexible, antistatic polyimides with low solar absorptivity for space applications.[1−8]

Although some properties of polymers can be affected by the addition of small amounts of SWNTs, properties such as improved thermal conductivity are expected to require much higher loadings, nanotube alignment, and perhaps modification to the interface between the nanotube and the matrix. This represents a major challenge as it is more difficult to disperse SWNTs at higher weight loadings. The advantage of dispersing SWNT bundles to smaller bundles or single nanotubes is that the SWNT surface area of these tubes is greatly increased and much more of the polymer matrix is affected by the SWNTs. A larger surface area creates a larger interfacial area, which in turn affects bulk properties of the composite. Thus, discovering new mechanisms for increasing the dispersion of SWNTs is one major driver for new technology in this area.

There have been many developments in the dispersion of SWNTs in both aqueous and organic solvents as well as in polymers. There are four prominent methods for achieving dispersion: mechanical methods,[8−10] functionalizing the SWNTs,[11−20] using surfactants,[21] and noncovalent modification by using small molecules and polymer dispersants.[22−40] There are advantages and disadvantages associated with each of the listed methods. For example, the use of mechanical means like high powered sonication or shearing forces to disperse SWNTs is effective but can decrease the length and consequently alter the properties of the SWNTs. Surfactants work extremely well in aqueous solutions but are ineffective in organic solvents. Functionalization of SWNTs is also a viable means to enhance dispersion, but this method changes the hybridization of the carbon atoms on the SWNTs, and thus the properties can also be changed. Perhaps the most effective means for dispersing SWNTs is the use of noncovalent modification, a technique that does not alter the properties of SWNTs. One potential disadvantage associated with noncovalent modification is that the dispersant must remain in the system to maintain dispersion. This may not be desirable since the dispersant can alter the properties of the final material, but if the dispersant has similar properties to the matrix or can serve as a matrix, then noncovalent modification can be very attractive.

We recently reported that noncovalent modification with ionomers prepared from AFDA and an aromatic bis(pyrylium salt) aided in dispersing SWNTs in organic solvents, and the ionomers/SWNT suspensions could subsequently be blended with polyimides.[41] Although the ionomers were useful, the associated difficulty in preparing the ionomers rendered them somewhat unattractive for practical use. Difficulty arose from the fact that monomers used to synthesize the ionomers were not commercially available, and the polymerization required high temperatures (165 °C). The purpose of the described work was to develop a dispersant for SWNTs that had similar dispersive properties as the previously reported ionomers but was more cost-effective and practical to prepare. A room temperature polymerization involving the use of the same diamine used for the ionomer synthesis and commercially available dianhydrides was used in the preparation of polyimides. Representative polyimides were prepared, and three polyimides were found to be effective dispersants for SWNTs.

† National Institute of Aerospace.
‡ NASA Langley Research Center.
* To whom correspondence should be addressed: e-mail john.w.connell@nasa.gov.

10.1021/ma051826u CCC: $33.50
Published on Web 02/09/2006

Suspensions containing up to 1 wt % SWNT in these polyimides were used to prepare films and electrospun fibers. The dispersion and orientation of SWNTs within the nanocomposites along with other select properties of these films are discussed herein.

2. Experimental Section

2.1. Starting Materials. Bucky Pearl SWNTs (lot no. PO222, 90% purity) were purchased from Carbon Nanotechnologies, Inc., and used as received. 2,3,3′,4′-Biphenyltetracarboxylic dianhydride (a-BPDA) was obtained from Ube Industries, Ltd., and recrystallized from a 1:1 mixture of toluene:acetic anhydride to yield white crystals (mp 196−198 °C). s-BPDA (Chriskev Co., mp 297−298 °C) and phthalic anhydride (PA) (Mallinkroft Specialty Chemical Co., mp 131 °C) were used as received. Pyromellitic dianhydride (PMDA) was obtained from Allco Chemical Corp. and sublimed to provide white sublimate (mp 284−286 °C). ODPA was obtained from Imitec, Inc., and sublimed to yield a white crystalline solid (mp 224−226 °C). 4,4′-Perfluoroisopropylidiene dianhydride (6FDA) was obtained from Hoechst Celanese, Inc., and sublimed prior to use (mp 241−243 °C). 4,4′-(4,4′-Isopropylidenediphenoxy)bis-(phthalic anhydride) (BPADA) was obtained from GE Plastics, Inc., and dried at 150 °C prior to use. 2,7-Diamino-9,9′-dioctylfluorene (AFDA) was prepared according to a literature procedure.[41] All other materials were purchased from commercial sources and used without further purification.

2.2. Preparation of High Molecular Weight (HMW) Polyimides. Into a 100 mL, three-necked flask equipped with nitrogen inlet, mechanical stirrer, and drying tube were placed AFDA (10.02 g, 23.8 mmol) and DMAc (50 mL). The mixture stirred until the diamine completely dissolved. ODPA (7.39 g, 23.8 mmol) was added as a powder followed by additional DMAc (30 mL) (18.8% solids). After the intermediate poly(amide acid) (PAA) stirred for ∼16 h, pyridine (5.65 g) and acetic anhydride (7.29 g) were added, and the solution was stirred for ∼16 h. DMAc (310 mL) was then added to the solution followed by 0.5 h of stirring. The solution was subsequently poured into water (2 L) in a Waring blender. The resulting powder was washed with water and dried by heating to 100 °C for 24 h.

2.3. Preparation of End-Capped, Low Molecular Weight Polyimides. Into a 500 mL, three-necked flask equipped with nitrogen inlet, mechanical stirrer, and drying tube were placed AFDA (11.50 g, 27.3 mmol) and DMAc (50 mL). The reaction mixture stirred until the diamine completely dissolved. s-BPDA (7.76 g, 26.4 mmol) and PA (0.2842 g, 1.9 mmol) were added as powders followed by additional DMAc (50 mL). After the reaction mixture stirred for ∼16 h, pyridine (6.49 g) and acetic anhydride (8.37 g) were added, and the solution was stirred for ∼16 h. DMAc (300 mL) was then added, and the solution was stirred for ∼0.5 h, after which the solution was poured into water (2 L) in a Waring blender. The resulting powder was washed with water and dried by heating at 100 °C for ∼24 h. The number-average molecular weight (M_n) was 9410 g/mol as determined by gel permeation chromatography (GPC).

2.4. Determination of Dispersant Effectiveness. Polyimides were screened for effectiveness at dispersing SWNTs at room temperature by the following method:

Into a 20 mL scintillation vial were placed SWNT (1.0 mg) and DMAc (5.0 g). The vial was submerged in a Branson 2510 Bransonic ultrasonic cleaner bath operating at 42 kHz for 10 min followed by the addition of the polyimide (20.0 mg). Sonication was administered for another 10 min, and the vial was then immediately removed from the bath and visually examined for appearance. The temperature of the sonicator bath was at ambient conditions and did not change significantly during these experiments. Effectiveness at breaking up SWNT agglomerates into small bundles was indicated by a visually homogeneous solution without any visual particulates.

2.5. Preparation of Polyimide/SWNT Mixtures. The following is a representative procedure for preparing polyimide/SWNT mixtures:

Into a 20 mL scintillation vial were placed SWNTs (10 mg) and DMAc (7.15 g). The suspension was sonicated in a Branson 2510 Bransonic ultrasonic cleaner bath operating at 42 kHz for ∼1 h followed by the addition of polyimide (0.1 g). The suspension was then subjected to ∼0.5 h sonication followed by two more polyimide additions of 0.2 g each with 10 min of sonication after each addition. The bath water reached temperatures of ∼45−55 °C after 1 h of sonication. A final polyimide addition (0.5 g) was then made, and the mixture was placed on a mechanical shaker for ∼3 h. The polyimide/SWNT mixtures were used to cast thin films.

2.6. Thin Films. Thin films were cast from control solutions (polymer only) and nanocomposite mixtures. The neat solutions and the nanocomposite mixtures were doctored onto plate glass and dried to a tack-free state under flowing nitrogen at room temperature in a low-humidity chamber. Solvent removal was done under flowing air after drying to a tack-free film as follows: 1 h each at 100, 200, and 0.5 h at 220 °C. Thin-film tensile properties were determined according to ASTM D882 at room temperature using five specimens from each film at a cross-head speed rate of 0.5 mm/min.

2.7. Electrospun Fibers. Nanocomposite mixtures (∼18% solids) were transferred to a 5 mL syringe which was placed in a syringe infusion pump (Fisher Scientific, Suwanee, GA). A high-voltage power supply (Spellman High Voltage Electronics Corp., Hauppage, NY) was used to charge the syringe tip to 28 V. The nanocomposite mixture was simultaneously pumped at a constant rate of 3.3 mL/h under the applied voltage. The charge on the mixture eventually overwhelmed its surface tension, and a jet was ejected from the needle tip to a grounded collector. The grounded collector in this setup was a spinning mandrel located 20 cm away from the syringe tip oriented parallel to the tip. The fibers were collected on the spinning mandrel, resulting in a fibrous mat.

2.8. Computational Modeling. Computational modeling of polyimide/carbon nanotube systems was performed in order to complement the experimental work. Carbon nanotubes were simulated in a polyimide matrix in full atomistic detail. The molecular modeling program LAMMPS[42,43] was used to perform the molecular dynamics and molecular mechanics energy minimization. The AMBER[44] force field was used with the molecular modeling. Periodic boundary conditions were used consistently with a final equilibrated box length size of about 40 Å. This periodic cell contained from 7000 to 8000 atoms, depending on whether the simulation was bulk polymer or nanocomposite. Because of the large aspect ratio, the nanotube was modeled as extending through the periodic boundary conditions. A (10,10) carbon nanotube was modeled consistently, with a radius of about 7.5 Å.

2.9. Characterization. High-resolution scanning electron microscopy (HRSEM) images were obtained on a Hitachi S-5200 field emission scanning electron microscopy system. Optical microscopy was performed using an Olympus BH-2 microscope at a magnification of 500×. Surface resistivity was determined according to ASTM D-257-99 using a Prostat PSI-870 surface resistance and resistivity indicator operating at 9 V and reported as an average of three readings. Volume resistivity was determined using a Prostat PRS-801 resistance system with a PRF-911 concentric ring fixture operating at 10−100 V according to ASTM D-257. Raman spectroscopy was performed using a Thermo Nicolet Almega dispersive Raman spectrometer equipped with a 785 nm laser. Inherent viscosities were obtained for 0.5% (w/v) solutions in DMAc at 25 °C. A Waters 150C GPC system was employed using an RI detector and a Viscotek viscometer. Waters Stryagel HT3, HT4, and HT6E size exclusion columns were hooked up in tandem and equilibrated with *N*-methyl-2-pyrrolidinone (NMP) (with 0.02 M LiBr) at a column temperature of 60 °C. The flow rate was set to 1 mL/min. A calibration curve was generated using polystyrene molecular weight standards from Polymer Laboratories. Samples were weighed out, and high-purity, anhydrous NMP (with 0.02 M LiBr) was added to each sample and shaken for several minutes to completely dissolve the sample. The samples were then filtered through a 0.2 μm syringe filter (PTFE filter matrix) to remove any insoluble material prior to injection on the column. A 100 μL sample

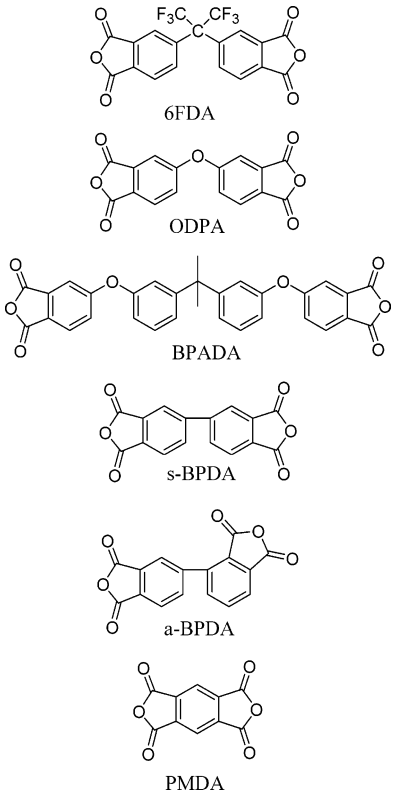

Figure 1. Dianhydrides used in comparison study.

Table 1. Properties of HMW Polyimides

sample	dianhydride	inherent viscosity (PAA) (dL/g)	soluble in DMAc at 25 °C
P1	s-BPDA	1.37	partially
P2	a-BPDA	1.14	yes
P3	ODPA	0.83	yes
P4	6FDA	0.65	yes
P5	BPADA	0.61	yes
P6	PMDA	0.52	partially

was injected into the column, and data were collected using Viscotek GPC software. Each sample was run in duplicate, and the data from each run were analyzed using the software to calculate the M_n and weight-average molecular weight (M_w) for each sample.

3. Results and Discussion

3.1. Preparation of Polyimides. Polyimides were prepared from AFDA and aromatic dianhydrides (Figure 1). Stoichiometric amounts of the monomers were used in the synthesis to achieve the highest molecular weight possible.

The poly(amide acid)s had inherent viscosities ranging from 0.52 to 1.37 dL/g (Table 1), indicating medium to high polymer formation. Solubility tests indicated that the corresponding polyimides (P2−P5) would readily dissolve in DMAc. P1 and P6 would only partially dissolve in DMAc when 20 mg of the polyimide was placed in 5 g. The reduced solubility can be explained by the more rigid dianhydrides used with P1 and P6.

To increase the solubility of the P1 polymer, a series of lower molecular weight oligomers having the same structure as P1 were prepared at 6.9% (EP1), 4.7% (EP2), and 3.5% (EP3) stoichiometric offset and end-capped with PA (Figure 2).

These imide oligomers were soluble in DMAc to at least 20 wt % solids and were characterized by GPC. The GPC data for the oligomers as well as for P3 are shown in Table 2.

3.2. Polyimide/SWNT Interactions and Preparation of Nanocomposites. The polyimides were then tested for their effectiveness in breaking up SWNT bundles in DMAc. Upon

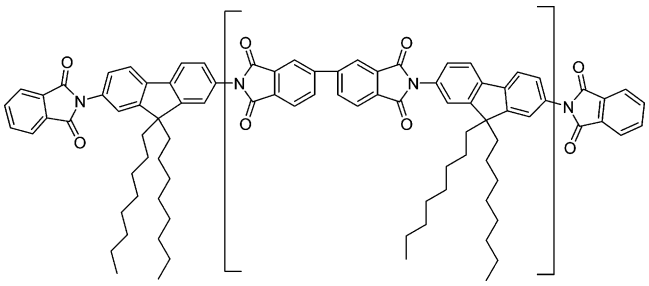

Figure 2. Imide oligomers from AFDA and s-BPDA.

Table 2. Properties of Controlled MW AFDA−s-BPDA Polyimides

sample ID	M_n (g/mol)	poly-disperity (PD)	intrinsic viscosity (dL/g)	soluble in DMAc at 25 °C
EP1	6860	2.3	0.25	yes
EP2	8250	2.3	0.33	yes
EP3	9410	2.0	0.44	yes
P3	17050	2.94	0.63	yes

Table 3. Polymer Effectiveness

sample	homogeneous suspension	sample	homogeneous suspension
P1	yes	P6	yes
P2	no	EP1	no
P3	yes	EP2	no
P4	no	EP3	partial
P5	no		

sonicating the neat SWNTs in DMAc, the SWNT chunks would swell, yielding visibly suspended agglomerates. After adding polyimide to the SWNT suspensions, the interaction between the polyimides and the SWNTs was visually observed. The result of a favorable interaction between polyimides and SWNTs was a homogeneous suspension devoid of any visible SWNT agglomerates, while unfavorable interactions resulted in SWNT suspensions with no effective change when compared to the neat samples. Data from the qualitative assessment of polyimide−SWNT interaction are recorded in Table 3.

Polymers P2, P4, P5, EP1, and EP2 exhibited unfavorable interactions once added to the suspensions as SWNT agglomerates were visually apparent. However, polymers P1, P3, and P6 exhibited favorable interactions with the SWNTs. Surprisingly, P1 and P6 were effective at breaking up the SWNT agglomerates even though these polyimides were only slightly soluble in DMAc. The difference in polymer/SWNT interaction between P1 and P2 was peculiar because the dianhydrides were isomers. The results indicate that proper alignment of the polymer with the nanotube could not be achieved when the asymmetric isomer of BPDA was used. This is consistent with findings that polymers with more bent isomers of BPDA exhibited weaker intermolecular interactions.[45]

The combination of polymer solubility with the ability to evenly distribute small SWNT bundles was necessary to prepare nanocomposite films from these polyimides. The initial screening studies indicated P3 to be the best choice. The results also indicated the EP3 polymer to be a good candidate. Although EP3 was not completely successful at creating homogeneous SWNT/solvent mixtures at the ratio used for the visual test (20 mg of polymer/1 mg of SWNT), suspensions with EP3 were much improved when compared to neat SWNT suspensions. It was assumed that higher polymer concentrations would yield completely homogeneous suspensions. This was later confirmed as homogeneous suspensions were afforded during film preparation. Higher MW polymers may have also proven successful, but EP3 was slow to dissolve and thus no attempt was made to use higher molecular weight versions for film preparation.

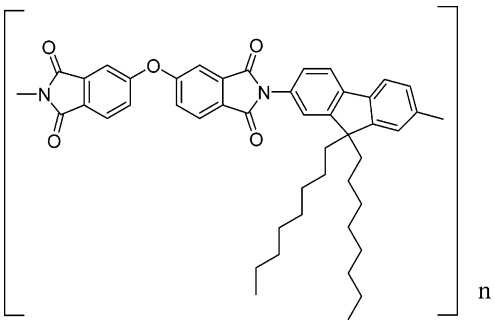

Figure 3. P3 polyimide.

3.3. Preparation of Nanocomposites. The other polymer chosen for nanocomposite preparation was the P3 polymer shown in Figure 3 and EP3 (see Figure 1).

The first step in preparing nanocomposites was to dissociate SWNT bundles in solvent via sonication. Additional sonication and agitation were administered after the polymer was added. Solutions containing 0.1, 0.5, and 1 wt % SWNT were then doctored onto glass and films prepared. In the case of polyimide P3, fibers were also prepared from the 1 wt % sample.

Raman spectroscopy showed similar results for these films compared to those obtained for previously prepared ionomer-based nanocomposites, and thus it was assumed that the chemistry of the SWNTs was unaffected during nanocomposite preparation.[41]

3.4. Optical and HRSEM Images of Nanocomposite Films. Visual examination of nanocomposite films revealed darker films as the SWNT loading level was increased. However, transparency was maintained in all the films except the 1 wt % P3 film, which was slightly hazy. Optical microscopy, which is generally used to visualize bundles and agglomerates of SWNTs, was used to further characterize the degree of SWNT dispersion in the nanocomposite films. Figure 4 confirms the presence of bundles, which appear as patterns of black lines, in all the EP3 films. The bundles are evenly distributed throughout the matrix in the 0.1 and 0.5 wt % EP3 films. However, agglomerates are noticeable in the 1% EP3 film, indicating incompleteness in breaking up the SWNT bundles. The P3 films (Figure 5) exhibited similar dispersion characteristics, but a few agglomerates were also noticed in the 0.5% SWNT loaded films. The optical microscopy data revealed that the EP3 polymer was better at dispersing SWNTs at higher loadings. This is most likely related to polymer structure as the lowering of the MW was shown to diminish the dispersing power of the polyimides.

HRSEM was also used to examine SWNT dispersion in the films. HRSEM images were taken while the film surface was oriented normal to the beam. The contrast between SWNTs and polymer is due to variations in the beam-induced electric field and allows for a direct assessment of SWNT dispersion within polymer matrices.[20,38] Obtaining HRSEM images was only possible for those films with sufficient conductivity to withstand exposure to the electron beam. Therefore, the 0.1% EP3 and P3 films could not be imaged. Although the 0.5% and 1% EP3 films were not highly conductive (Table 3), they exhibited unusually high stability in the beam at high voltages (20 kV). In all the films, SWNTs appeared to be uniformly distributed in arrays of ropelike networks. In both the 0.5% and the 1% EP3 samples, the SWNTs were randomly oriented with small bundle sizes (<10 nm) (Figure 6). Nearly identical images were obtained for the P3 nanocomposites, except that the 0.5% sample was not as stable under the electron beam. This is noticed in the darkening of the images and is consistent with the lower conductivity values obtained for the 0.5% P3 film than for the 0.5% EP3 film (section 3.5).

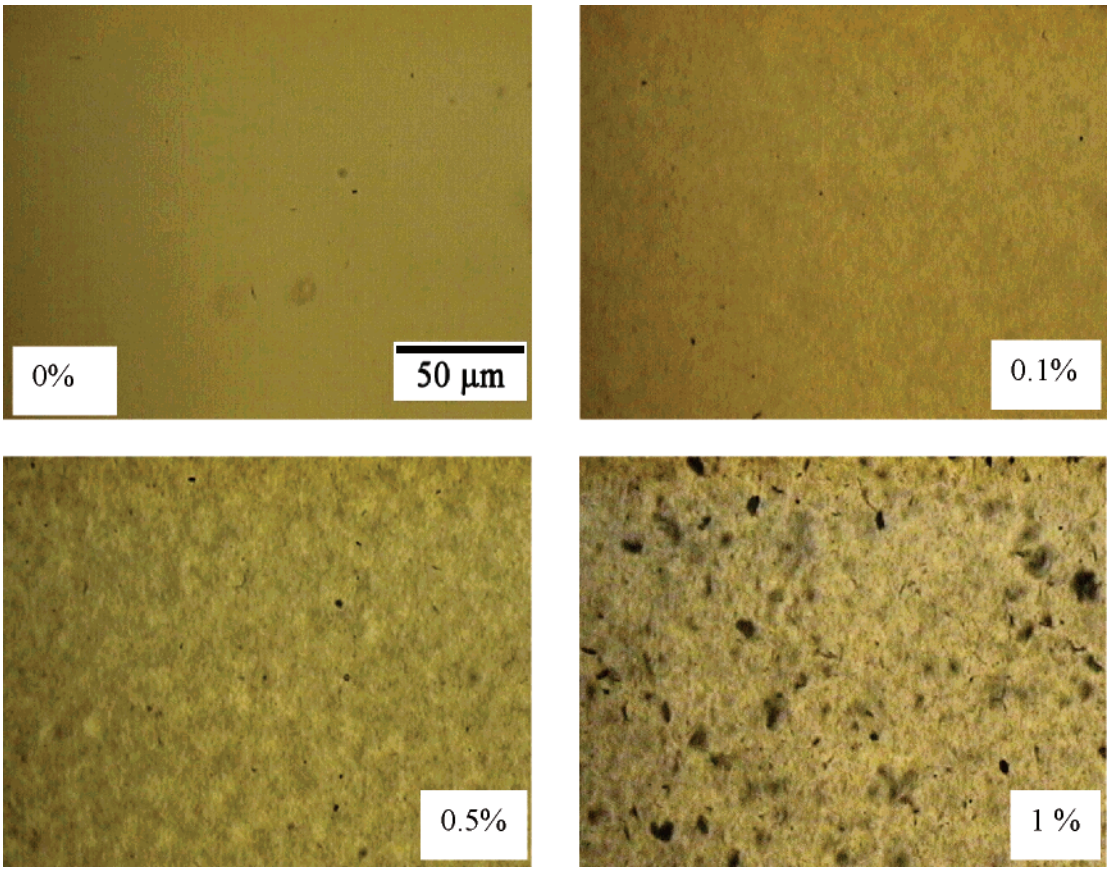

Figure 4. Optical microscopy of EP3 films (scale bar for all images in Figures 4 and 5).

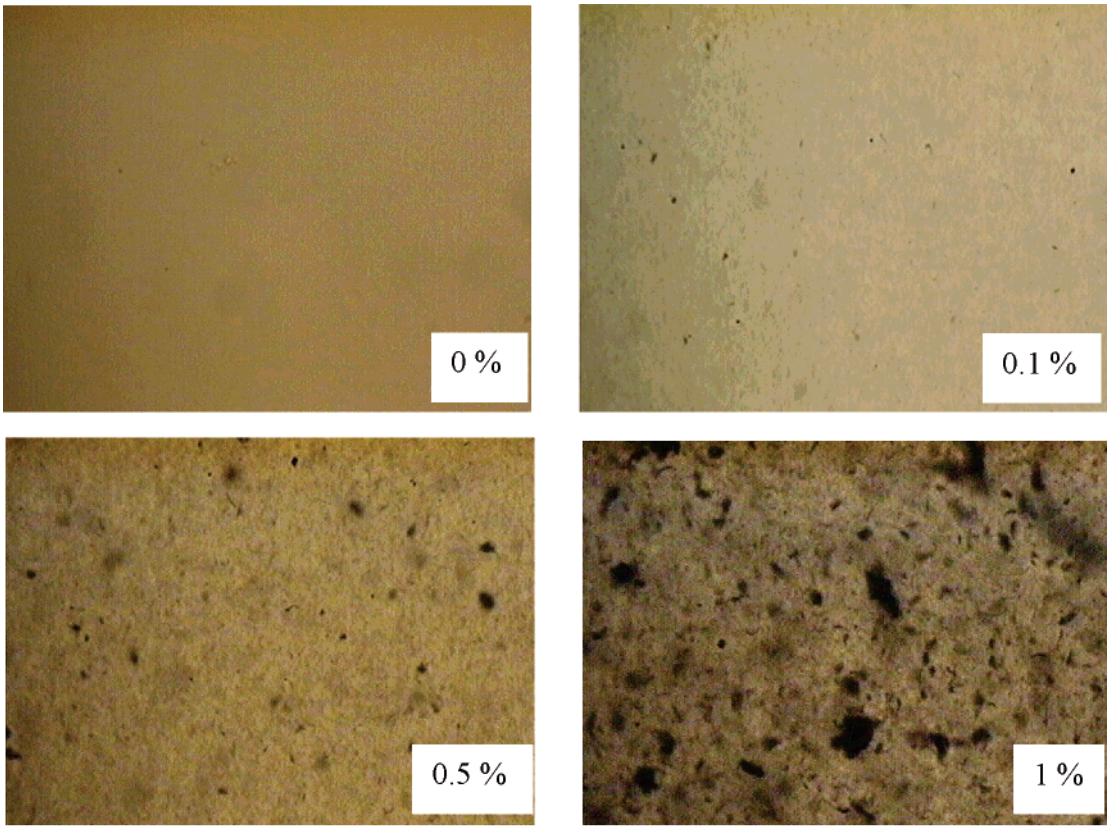

Figure 5. Optical microscopy of P3 nanocomposite films.

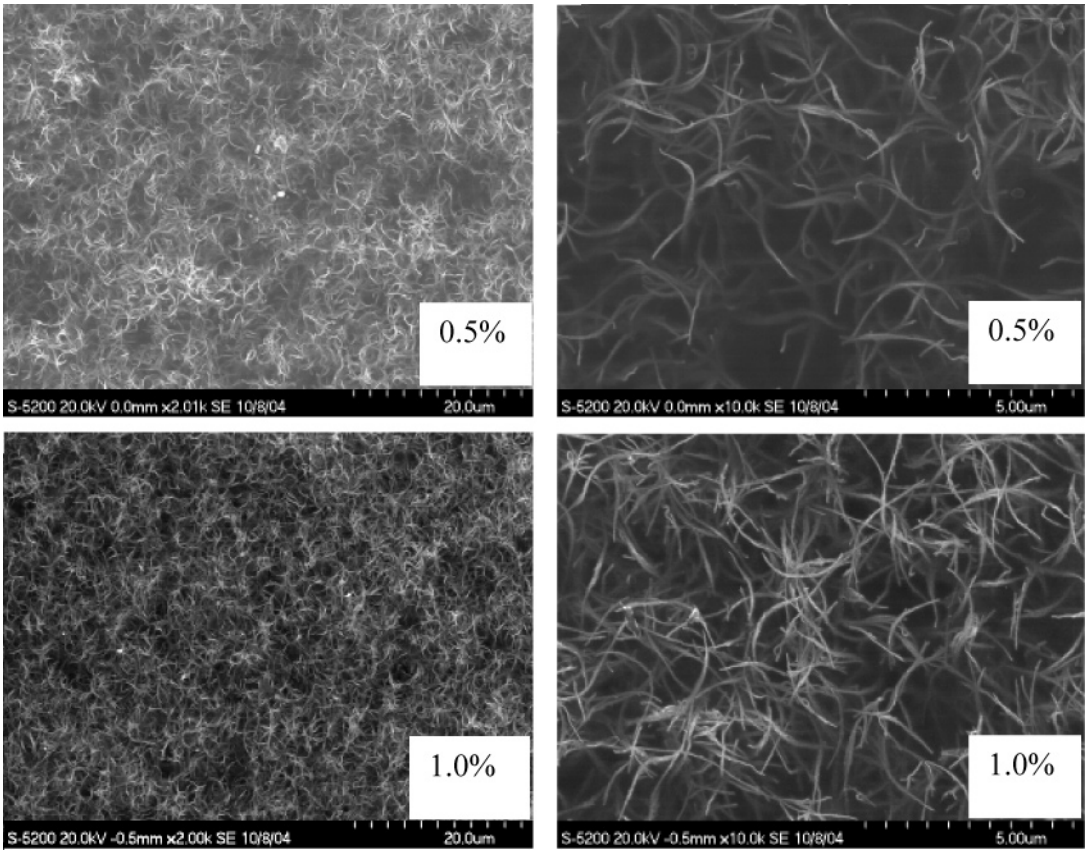

Figure 6. HRSEM images of EP3 nanocomposites.

3.5. Electrical Properties of Nanocomposite Films. Conductivity of polymer film can be affected by SWNT addition, and the percolation threshold usually occurs below 0.1 wt %.[1−8,46] The resistivity values for EP3 films and P3 films (Tables 4 and 5, respectively) show that percolation occurred above 0.1% in the case of EP3 and above 0.5% for the P3 films.

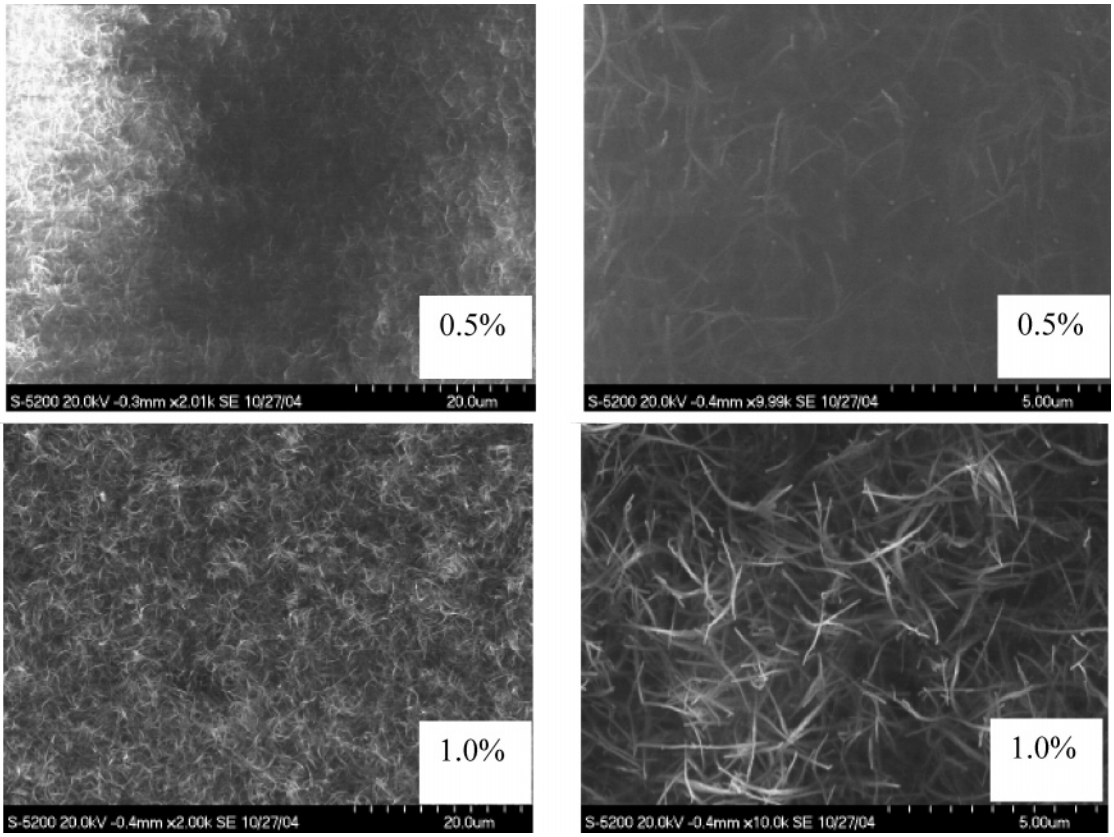

Figure 7. HRSEM images of P3 nanocomposites.

Table 4. Resistivity of EP3−SWNT Films

sample	SWNT loading (wt %)	surface resistivity (Ω/sq)	vol resistivity (Ω cm)
EP3	0	3.23×10^{12}	9.76×10^{14}
EP3	0.1	1.43×10^{12}	3.01×10^{13}
EP3	0.5	3.67×10^{9}	1.25×10^{10}
EP3	1	4.03×10^{7}	3.4×10^{9}

Table 5. Resistivity of P3−SWNT Films

sample	SWNT loading (wt %)	surface resistivity (Ω/sq)	vol resistivity (Ω cm)
P3	0	2.97×10^{12}	7.19×10^{14}
P3	0.1	2.01×10^{12}	7.86×10^{14}
P3	0.5	1.21×10^{12}	2.94×10^{14}
P3	1	3.97×10^{8}	6.16×10^{7}

The reason for the increased loading needed to reach percolation is not understood. However, one suggestion is that the high affinity of the polymer for the SWNT surface allows the polymers to completely coat and insulate the SWNT surface. Thus, the SWNTs and SWNT bundles are coated with the insulative polymer in such a way as to prevent the charge from transferring from one SWNT bundle to another. The change in percolation threshold could also be a result of the more uniform distribution of SWNT bundles, which in turn would decrease the likelihood of bundles touching to form a conductive network. The surface and volume resistivity values for the samples after reaching percolation are similar to those typically found in polyimide/SWNT films. For example, a previously prepared LaRC-CP2 film containing 0.05 wt % SWNT had a surface resistivity of 10^8 Ω/sq and a volume resistivity of 10^9 Ω cm.[7]

3.6. Tensile Properties of Nanocomposite Films. Tensile properties of polymer/SWNT nanocomposites depend on the orientation of SWNTs within each sample. For example, large increases in modulus and strength are reported if SWNTs are aligned,[47,48] but if random orientation is present, the mechanical properties are not improved by the addition.[43] Optical microscopy and HRSEM for both the P3 and EP3 films show very little SWNT alignment, and thus the nanocomposite films were not expected to show large increases in either tensile modulus or strength. However, moduli in both the P3 films and EP3 films (Tables 6 and 7, respectively) did increase slightly as the SWNT concentration increased. In both polymer systems there were only minor differences in film strength as a function of SWNT loading. Conversely, elongations of P3 nanocomposites were considerably altered. The reason for the sharp drop in elongation in the P3 nanocomposites is not clear but may be a result of stress concentration regions introduced by the nanotube bundles or larger agglomerates at higher weight loadings. This change in elongation was not noticed in the EP3 polymer perhaps because the neat sample had a low elongation to begin with.

Table 6. Room Temperature Thin Film Tensile Properties of EP3 Nanocomposites

sample	SWNT loading (wt %)	modulus (GPa)	strength (MPa)	elongation (%)
EP3	0	2.38 ± 0.07	72.3 ± 3.1	7 ± 1.5
EP3	0.1	2.41 ± 0.00	74.2 ± 1.4	6 ± 1.0
EP3	0.5	2.46 ± 0.03	77.1 ± 0.8	9 ± 0.5
EP3	1	2.61 ± 0.02	76.5 ± 2.4	7 ± 1.5

Table 7. Room Temperature Thin Film Properties of P3 Nanocomposites

sample	SWNT loading (wt %)	modulus (GPa)	strength (MPa)	elongation (%)
P3	0	1.57 ± 0.02	66.3 ± 3.3	49 ± 6.1
P3	0.1	1.58 ± 0.03	57.1 ± 0.8	16 ± 0.5
P3	0.5	1.73 ± 0.03	60.9 ± 1.4	21 ± 1.2
P3	1	1.71 ± 0.02	59.6 ± 1.1	14 ± 5.0

3.7. Computer Simulation of Polymer−Nanotube Systems. To examine the nature of the interaction between the polymer

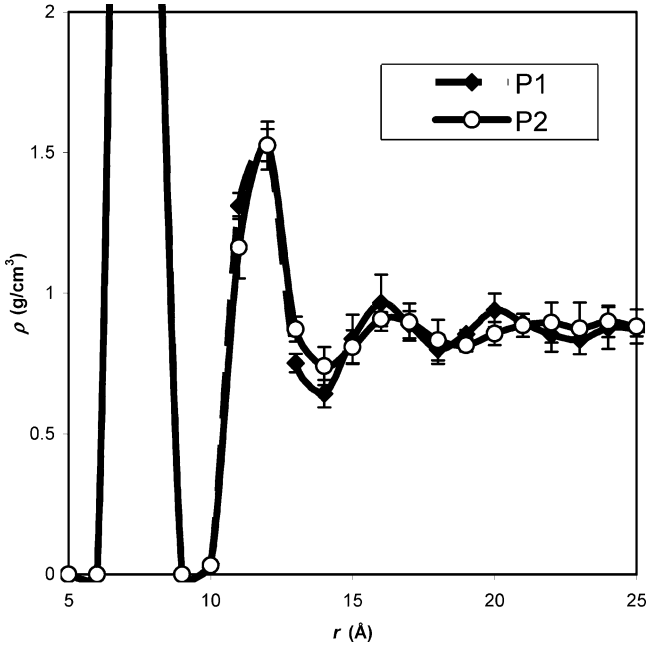

Figure 8. Radial density of the polymer/SWNT systems.

matrix and SWNTs, molecular dynamics (MD) simulations were performed. The experimental results indicate that P1 (s-BPDA) is able to evenly distribute SWNTs while the asymmetric isomer P2 (a-BPDA) does not. Since these two polymers are identical in chemical constituency, differing only in the geometry of the attachment about the biphenyl linkage, modeling was used to gain insight into the mechanisms influencing the different behavior of these two isomers with the SWNTs.

In the molecular modeling, nine chains of molecular weight 5400 g/mol each have been simulated with a 4 nm length section of a SWNT. These simulations were performed in fully atomistic detail with applied periodic boundary conditions. Three statistically independent models were prepared for each of the two polymer matrix types. The initial configurations were prepared by arranging the chains and the nanotube at low density and condensing the system with constant pressure MD. This was followed by 200 ps of constant pressure MD at 300 K. The same procedure was applied to generate bulk samples without the nanotube. Figure 8 shows the radial density of the polymer/nanotube system as a function of distance from the center of the nanotube. The large peak at 7−8 Å represents the SWNT wall. The data in this figure show that both polymers exhibit similar density profiles.

Energetics of the two nanocomposite systems were also studied using the following methodology. The comparative interfacial energy, $E_{\text{interface}}$, between the nanotube and the polymer for each polymer type is estimated from eq 1

$$E_{\text{interface}} = E_{\text{nanocomposite}} - E_{\text{nanotube}} - E_{\text{bulk polymer}} + E_{\text{tube extract}} \quad (1)$$

where $E_{\text{nanocomposite}}$ is the energy of the system with the nanotube embedded in the polymer, E_{nanotube} is the energy of the isolated nanotube, and $E_{\text{bulk polymer}}$ is the energy of the bulk polymer. $E_{\text{tube extract}}$ is the energy involved in extracting one nanotube from the middle of a system of a nanotube surrounded by six hexagonally packed nanotubes. This group of seven nanotubes is simulated in the same as way done for the polymer/nanotube system, where periodic boundary conditions are applied in the z direction along the axis of the tube. The comparative interfacial energy is converted to a surface energy in ergs/cm^2 by estimating the interfacial energy using a diameter of 10.5 Å. This value was chosen from consideration of Figure 8 and is arbitrarily but consistently applied. Results of the comparative interfacial energy calculation are shown in Table 8. The total energy is the sum of contributions due to the bond, angle, dihedral, improper, and nonbond terms. The dihedral energy of the s-BPDA/AFDA polymer is significantly lowered in the presence of the carbon nanotube, indicating that the s-BPDA isomer can adopt an energetically preferred conformation at the interface while the a-BPDA isomer does not. This would appear to be the primary influence for the results given in Table 3 with regard to these two isomers.

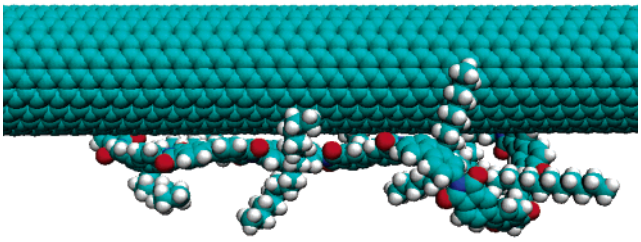

Figure 9. A single P1 chain in the presence of a SWNT illustrates how the polymer can adopt the preferred conformation.

Table 8. Comparative Interfacial Energies (erg/cm^2) for Two Polymer/Nanotube Systems Studied (P3 and EP3)

energy (erg/cm^2)	P2	P1
total	65	31
bond	1	6
angle	12	9
dihedral	−5	−59
improper	0	−1
nonbond	57	76

For illustration purposes, a short simulation of a single s-BPDA/AFDA polymer chain in the presence of a nanotube illustrates how the polymer can adopt the preferred conformation. This simulation was performed by removing eight of the chains from the bulk polymer/nanotube simulation, essentially exposing the polymer and the nanotube to vacuum. This results in the arrangement depicted in Figure 9 after ∼10 ps of MD simulation at 300 K. Attempts to generate a similar picture with the a-BPDA AFDA isomer resulted in the chain folding up and moving away from the tube.

3.8. Characterization of Electrospun Fibers. The 1 wt % P3 suspension that was used in film preparation was also used to prepare fibers by electrospinning. The fibers were collected as mats which had enough integrity to endure physical handling. Further mechanical property testing of the fibers was not considered due to the lack of proper testing equipment. However, conductivity of the fiber mat could be measured by a handheld conductivity meter, and the sample showed no increase in conductivity over the neat sample. However, a film prepared at the same wt % loading did show lowered resistivity (Table 5).

The orientation of SWNTs in the fibers was of interest, and the 1 wt % fiber was characterized by HRSEM. Upon analysis, it was observed that the fibers could withstand large voltages (20 kV) as in the case of more conductive films. This indicated that charge was dissipated by some mechanism not detectable with the conductivity meter. Although the 1% sample could withstand beam exposure, SWNTs could not be imaged inside the as-prepared fibers. Thus, a portion of the fiber mat was placed in an air oven at 350 °C for 1 h. After heating, the SWNTs were seen in the interior of the bundle (Figure 10), but at this concentration they did not appear to be completely aligned along the axis of the 1.5−2.0 μm fiber.

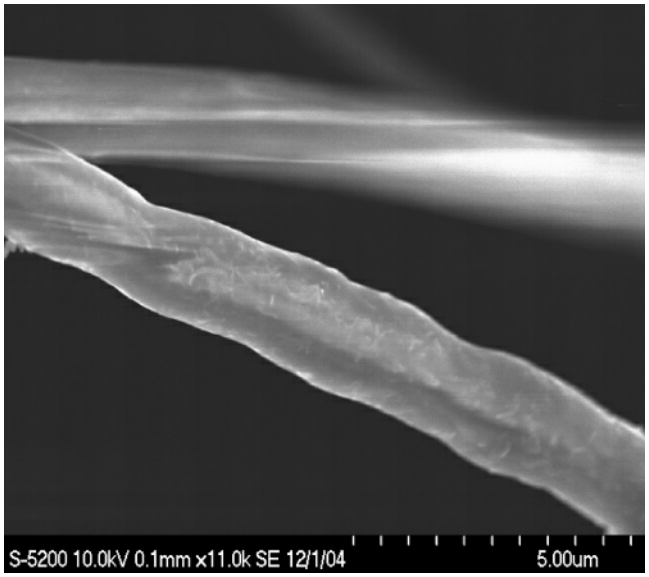

Figure 10. HRSEM image of electrospun fiber.

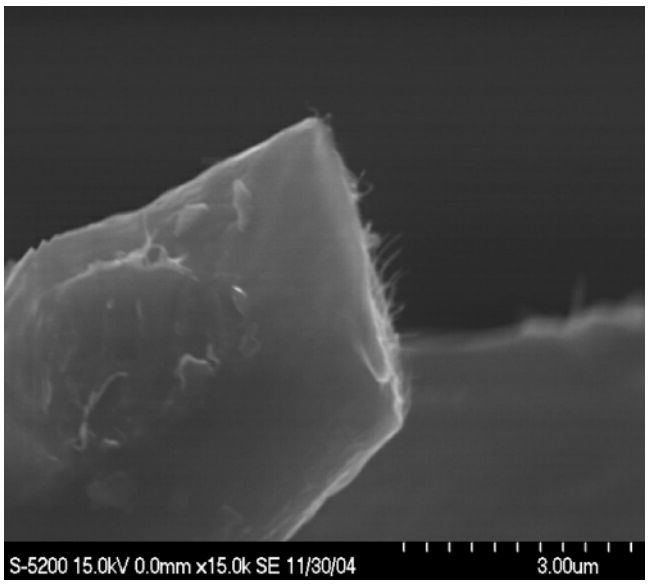

Figure 11. HRSEM showing fractured end.

The fibers were cut with a razor blade prior to imaging by HRSEM. SWNTs can be seen protruding at the fractured end and appear to be oriented parallel to the fiber axis (Figure 11).

4. Summary

Polyimides prepared with AFDA and various aromatic dianhydrides were tested for their effectiveness at dispersing SWNTs. Three polyimides were successful at breaking up SWNT agglomerates, resulting in homogeneous SWNT suspensions in DMAc. P1 was insoluble and required a reduction in molecular weight before films and fibers could be prepared. However, P3 was soluble at high molecular weight. Films prepared from both polyimides showed random distribution of small SWNT bundles by HRSEM. The SWNT bundles were not uniformly distributed in the 0.5 and 1 wt % P3 films and the 1 wt % EP3 film resulting in larger agglomerates. Increased electrical conductivity was seen in the nanocomposite films; however, electrical percolation occurred at higher loadings than are typically expected for polyimide/SWNT nanocomposites. Modulus of the films increased slightly with higher SWNT loading, though the strength of the films did not change as a function of SWNT loading. Elongation of the P3 films diminished as a result of SWNT loading. Electrospun fibers were prepared from the same polyimide/SWNT suspensions used to prepare the films. HRSEM showed that the SWNTs were captured in the interior of the fiber and may have some directionality parallel with the fiber axis.

References and Notes

(1) Watson, K. A.; Ghose, S.; Delozier, D. M.; Smith, J. G., Jr.; Connell, J. W. *Polymer* **2005**, *46*, 2076−2085.
(2) Watson, K. A.; Smith, J. G., Jr.; Connell, J. W. *Soc. Adv. Mater. Process Eng. Tech. Conf. Ser.* **2001**, *33*, 1551−1560.
(3) Smith, J. G., Jr.; Watson, K. A.; Thompson, C. M.; Connell, J. W. *Soc. Adv. Mater. Process Eng. Tech. Conf. Ser.* **2002**, *34*, 365−376.
(4) Smith, J. G., Jr.; Connell, J. W.; Lillehei, P.; Watson, K. A.; Thompson, C. M. *Mater. Res. Soc. Spring 2002 Session T, On-line Proc.* **2002**, *733E*, T3.5. www.mrs.org/publications/epubs/proceedings/spring2002/t/.
(5) Glatowski, P. J.; Connell, J. W.; Landis, D. H., Jr.; Smith, J. G., Jr.; Piche, J. W. U.S. Patent Application Publication 0164427, 2003.
(6) Smith, J. G., Jr.; Delozier, D. M.; Connell, J. W.; Watson, K. A. *Polymer* **2004**, *45*, 6133−6142.
(7) Delozier, D. M.; Watson, K. A.; Smith, J. G., Jr.; Connell, J. W. *Compos. Sci. Technol.* **2005**, *65*, 749−755.
(8) Park, C.; Ounaies, Z.; Watson, K. A.; Crooks, R. E.; Smith, J. G., Jr.; Lowther, S. E.; Connell, J. W.; Siochi, E. J.; Harrison, J. S.; St. Clair, T. L. *Chem. Phys. Lett.* **2002**, *364*, 303−308.
(9) Lin, T.; Bajpai, V.; Ji, T.; Dai, L. *Aust. J. Chem.* **2003**, *56*, 635−651.
(10) Mukhopadhyay, K.; Dwivedi, C. D.; Mathur, G. N. *Carbon* **2002**, *40*, 1373−1376.
(11) Chen, J.; Hamon, M. A.; Hu, H.; Chen, Y.; Rao, A. M.; Eklund, P. C.; Haddon, R. C. *Science* **1998**, *282*, 95−99.
(12) Niyogi, S.; Hamon, M. A.; Hu, H.; Zhao, B.; Bhowmik, P.; Sen, R.; Itkis, M. E.; Haddon, R. C. *Acc. Chem. Res.* **2002**, *35*, 1105−1113.
(13) Sun, Y. P.; Fu, K.; Lin, Y.; Huang, W. *Acc. Chem. Res.* **2002**, *35*, 1096−1104.
(14) Hill, D. E.; Lin, Y.; Rao, A. M.; Allard, L. F.; Sun, Y. P. *Macromolecules* **2002**, *35*, 9466−9471.
(15) Aizawa, M.; Shaffer, M. S. P. *Chem. Phys. Lett.* **2003**, *368*, 121−124.
(16) Banerjee, S.; Wong, S. S. *J. Am. Chem. Soc.* **2002**, *124*, 8940−8948.
(17) Bahr, J. L.; Tour, J. M. *Chem. Mater.* **2001**, *13*, 3823−3824.
(18) Dyke, C. A.; Tour, J. M. *J. Am. Chem. Soc.* **2003**, *125*, 1156−1157.
(19) Holzinger, M.; Abraham, J.; Whelan, P.; Graupner, R.; Ley, L.; Henrich, F.; Kappes, M.; Hirsch, A. *J. Am. Chem. Soc.* **2003**, *125*, 8566−8580.
(20) Smith, J. G., Jr.; Connell, J. W.; Delozier, D. M.; Lillehei, P. T.; Watson, K. A.; Lin, Y.; Zhou, B.; Sun, Y. P. *Polymer* **2004**, *45*, 825−836.
(21) Islam, M. F.; Rojas, E.; Bergey, D. M.; Johnson, A. T.; Yodh, A. G. *Nano Lett.* **2002**, *3*, 269−273.
(22) Star, A.; Liu, Y.; Gant, K.; Ridvan, L.; Stoddart, J. F.; Steuerman, D. W.; Diehl, M. R.; Boukai, A.; Heath, J. R. *Macromolecules* **2003**, *36*, 553−560.
(23) Chen, R. J.; Zhang, Y.; Wang, D.; Dai, H. *J. Am. Chem. Soc.* **2001**, *123*, 3838−3839.
(24) Star, A.; Steuerman, D. W.; Heath, J. R.; Stoddart, J. F. *Angew. Chem., Int. Ed.* **2002**, *41*, 2508−2512.
(25) Hirsch, A. *Angew. Chem., Int. Ed.* **2002**, *41*, 1853−1859.
(26) Ago, H.; Shaffer, M. S. P.; Ginger, D. S.; Windle, A. H.; Friend, R. H. *Phys. Rev. B: Condens. Matter Mater. Phys.* **2000**, *61*, 2286−2290.
(27) O'Connell, M. J.; Boul, P.; Ericson, L. M.; Huffman, C.; Wang, Y.; Haroz, E.; Kuper, C.; Tour, J.; Ausman, K. D.; Smalley, R. E. *Chem. Phys. Lett.* **2001**, *342*, 265−271.
(28) Curran, S.; Ajayan, P. M.; Blau, W. J.; Carroll, D. L.; Coleman, J. N.; Dalton, A. B.; Davey, A. P.; Drury, A.; McCarthy, B.; Maier, S.; Stevens, A. *Adv. Mater.* **1998**, *10*, 1091−1093.
(29) Coleman, J. N.; Dalton, A. B.; Curran, S.; Rubio, A.; Davey, A. P.; Drury, A.; McCarthy, B.; Lahr, B.; Ajayan, P. M.; Roth, S.; Barklie, R. C.; Blau, W. J. *Adv. Mater.* **2000**, *12*, 213-216.
(30) Curran, S.; Davey, A. P.; Coleman, J. N.; Dalton, A. B.; McCarthy, B.; Maier, S.; Drury, A.; Gray, D.; Brennan, M.; Ryder, K.; La Chapelle, M. L.; Journet, C.; Bernier, P.; Bryne, H. J.; Carroll, D.; Ajayan, P. M.; Lefrant, S.; Blau, W. *Synth. Met.* **1999**, *103*, 2559.
(31) McCarthy, B.; Coleman, J. N.; Czerw, R.; Dalton, A. B.; Carroll, D. L.; Blau, W. J. *Synth. Met.* **2001**, *121*, 1225−1226.
(32) Dalton, A. B.; Stephan, C.; Coleman, J. N.; McCarthy, B.; Ajayan, P. M.; Lefrant, S.; Bernier, P.; Blau, W. J.; Bryne, H. J. *J. Phys. Chem. B* **2000**, *104*, 10012−10016.

(33) Steuerman, D. W.; Star, A.; Narizzano, R.; Choi, H.; Ries, R. S.; Nicolini, C.; Stoddart, J. F.; Heath, J. R. *J. Phys. Chem. B* **2002**, *106*, 3124−3130.
(34) Wise, K. E.; Park, C.; Siochi, E. J.; Harrison, J. S. *Chem. Phys. Lett.* **2004**, *391*, 207−211.
(35) Star, A.; Stoddart, J. F.; Steuerman, D. W.; Diehl, M.; Boukai, A.; Wong, E. W.; Yang, X.; Chung, S. W.; Choi, H.; Heath, J. R. *Angew. Chem., Int. Ed.* **2001**, *40*, 1721−1725.
(36) Xu, H.; Tang, B. Z. *Polym. Mater. Sci. Eng.* **1999**, *80*, 408.
(37) Wang, J.; Musameh, M.; Lin, Y. *J. Am. Chem. Soc.* **2003**, *125*, 2408−2409.
(38) Landi, B. J.; Raffaelle, R. P.; Heben, M. J.; Alleman, J. L.; VanDerveer, W.; Gennett, T. *Nano Lett.* **2002**, *2*, 1329−1332.
(39) Fukushima, T.; Kosaka, A.; Ishimura, Y.; Yamamoto, T.; Takigawa, T.; Ishii, N.; Aida, T. *Science* **2003**, *300*, 2072−2074.
(40) Viswanathan, G.; Charapani, N.; Yang, H.; Wei, B.; Chung, H.; Cho, K.; Ryu, C.; Ajayan, P. M. *J. Am. Chem. Soc.* **2003**, *125*, 9528−9259.
(41) Delozier, D. M.; Tigelaar, D. M.; Watson, K. A.; Smith, J. G., Jr.; Lillehei, P. T.; Connell, J. W. *Polymer* **2005**, *46*, 2506−2521.
(42) Plimpton, S. J. *J. Comput. Phys.* **1995**, *117*, 1−19.
(43) http://www.cs.sandia.gov/~sjplimp/lammps.html.
(44) Cornell, W. D.; Cieplak, P.; Bayly, C. I.; Gould, I. R.; Merz, K. M.; Ferguson, D. M.; Spellmeyer, D. C.; Fox, T.; Caldwell, J. W.; Kollman, P. A. *J. Am. Chem. Soc.* **1995**, *117*, 5179−5197.
(45) Zhou, H.; Chen, C.; Kanbara, R.; Sasaki, T.; Yokota, R. *High Perform. Polym.* **2005**, *17*, 213−224.
(46) Shaefer, D. W.; Zhao, J.; Brown, J. M.; Anderson, D. P.; Tomlin, D. W. *Chem. Phys. Lett.* **2003**, *375*, 369−375.
(47) Siochi, E. J.; Working, D. C.; Park, C.; Lillehei, P. T.; Rouse, J. H.; Topping, C. C.; Bhattacharyya, A. R.; Kumar, S. *Composites: Part B* **2004**, *35*, 439−446.
(48) Uchida, T.; Kumar, S. *J. Appl. Polym. Sci.* **2005**, *98*, 985−989.

MA051826U